Enhanced closure scheme for lattice Boltzmann equation hydrodynamics

2002 J. Phys. A: Math. Gen. 35 L157

(http://iopscience.iop.org/0305-4470/35/12/102)

INSTITUTE OF PHYSICS PUBLISHING JOURNAL OF PHYSICS A: MATHEMATICAL AND GENERAL

J. Phys. A: Math. Gen. **35** (2002) L157–L166 PII: S0305-4470(02)31774-8

LETTER TO THE EDITOR

Enhanced closure scheme for lattice Boltzmann equation hydrodynamics

I Halliday, L A Hammond and C M Care

Materials Research Institute, Sheffield Hallam University, Howard Street, Sheffield S1 1WB, UK

Received 5 December 2001
Published 15 March 2002
Online at stacks.iop.org/JPhysA/35/L157

Abstract

A simple and adaptable *closure* algorithm for the edge nodes of a lattice Boltzmann fluid simulation space is presented. Its rules are designed to be correct at every instant, to maintain local mass and to produce a specified fluid velocity and, *crucially*, the correct strain rate tensor at the resulting fluid boundary. Further, our algorithm models the fluid on boundary nodes to the same accuracy as on the bulk nodes and in a demonstrably equivalent manner, requiring only a specified boundary velocity, the fluid boundary pressure emerging. Illustrative results for steady and time-dependent flows, together with outline generalizations, are presented.

PACS numbers: 47.45.−n, 02.60.−x, 05.50.+q

1. Introduction

Accurate representation of the boundary is as essential and complicated in lattice Boltzmann (LB) calculation as it is in any other branch of computational fluid dynamics. Our aim here is to extend transparently and verifiably the scope of the LB method, to implement accurately the boundaries which condition physical flows. In particular, for time-developing flows, our lattice closure strategy can be accurate over a very small number of simulation time steps and it is applicable to all flat boundaries over which there is a target distribution of velocity. Therefore our method can, in principle, be used to represent open or closed fluid boundaries not just no-slip boundaries.

The particular problems encountered by simulators of course depend upon the specific geometry of the LB simulation lattice, the particular LB algorithm and the type of boundary required. In general however, there are, in the literature, a number of methods for closing a simulation lattice, from which *emerge* the effective boundary conditions controlling the lattice fluid.

In application the simplest closure strategy is the device of *equilibrium forcing*, which involves persistently over-writing LB boundary nodes with the appropriate equilibrium momentum density distribution. Whilst robust, this method, at its simplest, is of first-order

accuracy. Again straightforward and robust, but only first-order accurate, is the widely used *bounce-back* rule (see e.g. [12]). Bounce-back enforces an equilibrium distribution function different from that of the core (bulk) scheme, resulting in a small slip velocity which varies with the value of the LB collision parameter [13]. These first-order closure strategies are not designed to be correct at every instant but some of their other idiosyncrasies are understood. For example bounce-back has been carefully evaluated at steady state by a number of workers (e.g. [2,9]) and He *et al* [5] have shown how it is possible to predict analytically *boundary slip velocities*.

Higher-order accuracy LB boundary algorithms involve bouncing back the non-equilibrium part of the LB momentum densities [12], extrapolation [1], the introduction of a counter-slip velocity [7] and second-order bounce-back [8], and Skordos [11] has solved the problem of boundary closure by deriving auxiliary partial differential equations which may be solved for lattice boundary information.

Of particular importance to the present work is what is possibly the most overlooked and most general approach to simulation lattice closure, the locally second-order boundary (LSOB) method of Ginzbourg and d'Humières [3] to which we shall return in section 3.

Fluid pressure and velocity both emerge from solutions of the Navier–Stokes and continuity equations given only the Dirichlet boundary conditions on fluid velocity:

$$\boldsymbol{v}(\boldsymbol{r}, t)|_{\boldsymbol{r}'} = \boldsymbol{u}_0(\boldsymbol{r}', t) \tag{1}$$

where $\boldsymbol{r}'$ denotes a position on the boundary of the fluid domain and $\boldsymbol{u}_0(\boldsymbol{r}', t)$ is a specified boundary velocity function. This boundary information alone is sufficient to close a particular solution of the governing equations.

In this letter, we derive and bench-test simple and adaptable *closure* rules for the edges of an LB fluid simulation space. These rules are equivalent to Dirichlet boundary conditions in that they aim to give correct fluid behaviour at every time-step, they are derived to model boundary lattice fluid at the accuracy of bulk lattice fluid and they require only a target velocity distribution whilst allowing boundary pressure to emerge. We treat in detail what is perhaps the most useful situation, a locally flat wall at which fluid is entrained with a specified velocity. However our analysis is applicable to other cases (vertical and inclined walls) provided certain conditions are met (see below).

It is henceforth assumed that a node designated a boundary lies infinitesimally *within* the lattice fluid and we thus suppose this node to be fully occupied by fluid moving at specified velocity. According to the above remarks, the momentum densities, f_i which comprise such a boundary shall be constructed by requiring that they evolve according to rules equivalent to those operating on bulk nodes.

2. Preliminary analysis

We take as an illustrative example the two-dimensional, nine-velocity (D2Q9) LBGK model (figure 1) pioneered by Qian *et al* [10] and analysed in detail by Hou *et al* [6]. However, it should be noted that our analysis will generalize directly to any scheme with a locally flat boundary. We denote all vectors of the lattice velocity basis by $\boldsymbol{c}_i$, with the indexing of figure 1. Collision and subsequent propagation of the D2Q9 LBGK model is given by

$$f_i(\boldsymbol{r} + \boldsymbol{c}_i\delta_t, t + \delta_t) = f_i(\boldsymbol{r}, t) + \frac{1}{\tau}(f_i^{(0)} - f_i), \tag{2}$$

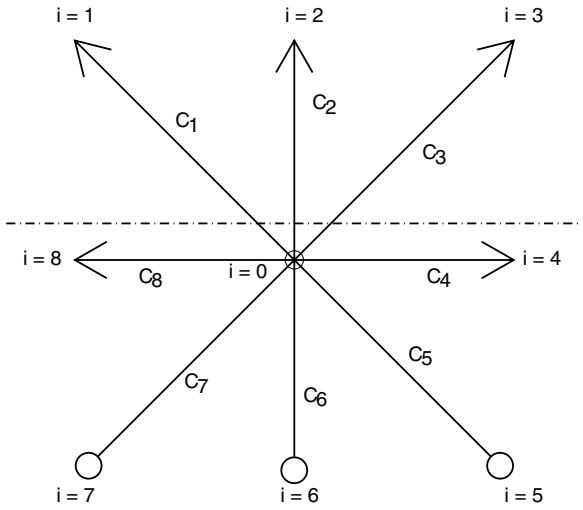

Figure 1. Schematic of a boundary node on the top wall, immediately prior to the collision step. Here the wall location is denoted by the dashed line, which makes the node 'infinitesimally wet'. Propagated data are denoted by arrowheads, unknown link information (lack of data) is denoted by the open circles on links. The links are numbered as referred to in the text and link velocity vectors are numbered accordingly.

where the parameter δ_t represents the time step and the collision scalar, τ, determines the fluid viscosity through

$$\nu = \frac{2\tau - 1}{6}\delta_t, \tag{3}$$

where $0 < 1/\tau < 2$ and all other symbols have their usual meaning [6, 10]. The macroscopic fluid density and momentum are defined by

$$\begin{aligned} \rho &= \sum_i f_i \\ \rho\, \boldsymbol{v} &= \sum_i f_i\, \boldsymbol{c}_i \end{aligned} \tag{4}$$

and the equilibrium distribution function, $f_i^{(0)}$, is chosen to be

$$f_i^{(0)}(\rho, \boldsymbol{v}) = t_p \rho \left[1 + \frac{\boldsymbol{v}\cdot\boldsymbol{c}_i}{c_s^2} - \frac{v^2}{2c_s^2} + \frac{(\boldsymbol{v}\cdot\boldsymbol{c}_i)^2}{2c_s^4} \right]. \tag{5}$$

In equation (5), the *weights* $t_p = 4/9, 1/9, 1/36$ for $i = 0$, i even, i odd respectively (figure 1) and $c_s = 1/\sqrt{3}$ is the velocity of sound, for the D2Q9 lattice. The choice of equilibrium distribution function, (5), gives

$$\begin{aligned} \rho &= \sum_i f_i^{(0)}, \\ \rho \boldsymbol{v} &= \sum_i \boldsymbol{c}_i f_i^{(0)} \end{aligned} \tag{6}$$

and also recovers the non-viscous pressure tensor:

$$\Pi_{\alpha\beta}^{(0)} = \sum_i f_i^{(0)} c_{i\alpha} c_{i\beta} = \tfrac{1}{3}\rho\delta_{\alpha\beta} + \rho v_\alpha v_\beta. \tag{7}$$

The higher-order contributions to the distribution function, $f_i^{(n)}$, are defined through the Chapman Enskog expansion [6]:

$$f_i = f_i^{(0)} + \delta_t f_i^{(1)} + \delta_t^2 f_i^{(2)} + \delta_t^3 f_i^{(3)} \cdots \tag{8}$$

and equation (6) ensures that

$$\sum_i f_i^{(n)} \Delta_i = 0 \qquad n > 0, \tag{9}$$

where $\Delta_i = 1, c_{ix}, c_{iy}$.

However, the second velocity moments of the $f_i^{(n)}$ are not zero. In particular, it can be shown from the Chapman Enskog analysis that

$$\sum_i f_i^{(1)} c_{i\alpha} c_{i\beta} = -2c_s^2 \rho \tau S_{\alpha\beta} \tag{10}$$

where $S_{\alpha\beta}$ is the rate of strain. We note that since $S_{\alpha\beta}$ is symmetric, equations (9) and (10) provide six equations constraining the $f_i^{(1)}$ and these equations are central to the method described in the next section.

3. Lattice closure algorithm

The problem of terminating the lattice resides in the fact that, in two dimensions, a *given* lattice fluid boundary node velocity provides only two conditions on moments of the f_i (through equations (4)), whilst there may be several unknown distribution functions f_i.

Figure 1 shows the boundary site on the D2Q9 lattice which we now analyse. The dotted line shows the supposed extent of the lattice fluid, links indexed $i = 1, 2, 3$ are 'cut' and the remaining links are taken to lie within the simulation domain. All the nodes other than the boundary nodes are evolved according to (2). At the end of a propagation step it therefore follows that on the boundary node shown in figure 1, a pre-collision value of lattice momentum density, f_i, exists for all links except $i = 5, 6, 7$ (indicated by circles as opposed to arrows).

However, it is necessary to consider more than the three unknown densities f_5, f_6 and f_7. The $f_i^{(0)}$ need to satisfy the three equations (6) and the $f_i^{(1)}$ need to satisfy *six* equations (9), (10) if we are to produce a closure algorithm which recovers velocities and velocity gradients which are correct at very short timescales.

Accordingly we set out to construct second-order correct f_i ($f_i^{(0)}$ and $f_i^{(1)}$) by determining the value of the $f_i^{(1)}$ on a set of six links at a boundary node (not just links $i = 5, 6, 7$), whilst allowing the lattice-edge density (pressure) to emerge from local information only, thus preserving an appropriate coupling between the boundary nodes and the bulk. Here we are assisted by the fact that the momentum and the wall node density uniquely determine $f_i^{(0)}$, whilst the viscous stress can be used separately to fix the $f_i^{(1)}$ through equation (10). The pre-collision boundary node densities thus constructed may then be collided and propagated. Our boundary node evolution thus involves the collision of second-order accurate f_i, which are consistent with the target boundary velocity *and* the implicit wall stress.

The idea of constructing the unknown momentum densities f_i by separately evaluating the individual contributions in the Chapman Enskog expansion (8) is, apparently, used by Ginzbourg and d'Humières [3], who consider a linearized LB equation model, both with flat and inclined Dirichlet boundaries, and show how, and under what circumstances the first- and second-order terms $f_i^{(1)}$ and $f_i^{(2)}$ may be evaluated from a set of first- and second-order velocity derivatives. By contrast we proceed via an alternative, we hope transparent, formulation to a simplified but more accessible analysis in which, for the equilibrium component of the unknown momentum densities, $f_i^{(0)}$ may always be evaluated directly (see below) and the first-order

corrections $f_i^{(1)}$ from the instantaneous boundary stress are solved explicitly in terms of the known $f_i^{(1)}$.

Our boundary scheme has the following principal steps:

(1) Determine the wall-node density, ρ, and hence the equilibrium momentum density distribution $f_i^{(0)}$, $i = 0 \ldots 8$ corresponding to the chosen boundary velocity using (5) (for all LBE schemes, $f_i^{(0)}$ is a function of velocity and density alone).
(2) Construct the appropriate pre-collision $f_i^{(1)}$ to recover the measured boundary node strain rates. It is actually necessary to determine at least six of the pre-collision $f_i^{(1)}$ (see below) in order to respect all the necessary conditions on the $f_i^{(1)}$.
(3) Collide and propagate the boundary sites according to equation (2).

We proceed now to detail steps (1)–(3) above. In step (1), the problem in determining the node density ρ is that the momentum densities, f_i, in the directions $i = 5, 6, 7$ are each unknown. However we can obtain an expression for their sum by considering the y-momentum, using (4):

$$f_1' + f_2' + f_3' - f_5 - f_6 - f_7 = \rho u_{0y} \tag{11}$$

where the primed momentum densities indicate known values, streamed from adjacent lattice sites at the previous time step, and u_{0y} is the target wall velocity, also known. The target density at the site is likewise expressed as a sum of known and unknown momentum densities:

$$f_0' + f_1' + f_2' + f_3' + f_4' + f_5 + f_6 + f_7 + f_8' = \rho. \tag{12}$$

Now it is possible to eliminate the term $(f_5 + f_6 + f_6)$ in the unknown densities between (11) and (12) to obtain an expression for ρ in terms of the *known* momentum densities:

$$\rho = \frac{1}{1 - u_{0y}}[f_0' + f_4' + f_8' + 2\,(f_1' + f_2' + f_3')]. \tag{13}$$

So, whilst the unspecified momentum densities f_5, f_6 and f_7 cannot be determined individually from a given boundary velocity, their sum, and hence the node density (pressure) *can*. With a value for the boundary node density, ρ, and the given boundary velocity it is possible directly to determine $f_i^{(0)}$ on all links using equation (5).

Step (2). Having established the equilibrium distributions, $f_i^{(0)}$, to recover the required density and momentum on the boundary nodes, the $f_i^{(1)}$ are chosen to recover the measured value of the rate of strain tensor, $S_{\alpha\beta}$. Hence the nine $f_i^{(1)}$, $i = 0 \ldots 8$ are chosen to satisfy the six equations given by (9) and (10):

$$\begin{aligned}
&f_0^{(1)} + f_1^{(1)} + f_2^{(1)} + f_3^{(1)} + f_4^{(1)} + f_5^{(1)} + f_6^{(1)} + f_7^{(1)} + f_8^{(1)} = 0,\\
&-f_1^{(1)} + f_3^{(1)} + f_4^{(1)} + f_5^{(1)} - f_7^{(1)} - f_8^{(1)} = 0,\\
&f_1^{(1)} + f_2^{(1)} + f_3^{(1)} - f_5^{(1)} - f_6^{(1)} - f_7^{(1)} = 0,\\
&f_1^{(1)} + f_3^{(1)} + f_4^{(1)} + f_5^{(1)} + f_7^{(1)} + f_8^{(1)} = -2\rho\tau/3\ \ S_{xx},\\
&f_1^{(1)} + f_2^{(1)} + f_3^{(1)} + f_5^{(1)} + f_6^{(1)} + f_7^{(1)} = -2\rho\tau/3\ \ S_{yy},\\
&-f_1^{(1)} + f_3^{(1)} - f_5^{(1)} + f_7^{(1)} = -2\rho\tau/3\ \ S_{xy}.
\end{aligned} \tag{14}$$

The velocity gradients which appear in the right-hand side of the last three of equations (14) above may be measured at the boundary using second-order accurate finite-difference expressions.

The solution of the above system (14) of simultaneous equations for the $f_i^{(1)}$ is complicated by the fact that it is under-determined. It is therefore necessary to select three $f_i^{(1)}$ to be

Table 1. Diagrammatic representation of the forbidden $f_i^{(1)}$ combinations.

Forbidden combinations	Link representation
$f_1^{(1)}, f_2^{(1)}, f_3^{(1)}$	
$f_3^{(1)}, f_4^{(1)}, f_5^{(1)}$	
$f_5^{(1)}, f_6^{(1)}, f_7^{(1)}$	
$f_1^{(1)}, f_7^{(1)}, f_8^{(1)}$	
$f_0^{(1)}, f_4^{(1)}, f_8^{(1)}$	
$f_0^{(1)}, f_2^{(1)}, f_6^{(1)}$	
$f_0^{(1)}, f_1^{(1)}, f_5^{(1)}$	
$f_0^{(1)}, f_3^{(1)}, f_7^{(1)}$	

free variables, with values chosen arbitrarily in order to fix those of the remaining six *basic* variables. However, the choice of free variables is restricted, since the determinant of the matrix of coefficients of the basic variables vanishes for certain choices of free $f_i^{(1)}$. We list, in column 1 of table 1, what we designate *forbidden combinations* of the free variables, obtained by considering this determinant for all possible choices of free variables. The table also includes a diagrammatic interpretation, relative to figure 1, of these forbidden sets of free variables.

We may further understand the origin of these forbidden combinations in the model symmetry if we consider the variable set

$$\begin{aligned}
g_1 &\equiv f_1^{(1)} + f_2^{(1)} + f_3^{(1)} \\
g_2 &\equiv f_5^{(1)} + f_6^{(1)} + f_7^{(1)} \\
g_3 &\equiv f_3^{(1)} + f_4^{(1)} + f_5^{(1)} \\
g_4 &\equiv f_1^{(1)} + f_7^{(1)} + f_8^{(1)} \\
g_5 &\equiv f_0^{(1)} + f_4^{(1)} + f_8^{(1)} \\
g_6 &\equiv f_0^{(1)} + f_2^{(1)} + f_6^{(1)} \\
g_7 &\equiv -f_0^{(1)} + f_1^{(1)} + f_5^{(1)} \\
g_8 &\equiv -f_0^{(1)} + f_3^{(1)} + f_7^{(1)}.
\end{aligned} \tag{15}$$

We may then write the system of equations (14) in the simplified form

$$\begin{aligned}
g_1 + g_2 \qquad\qquad + g_5 \qquad\qquad &= 0 \\
\qquad g_3 - g_4 \qquad\qquad &= 0 \\
g_1 - g_2 \qquad\qquad &= 0 \\
\qquad g_3 + g_4 \qquad\qquad &= -2\rho\tau/3\ S_{xx} \\
g_1 + g_2 \qquad\qquad &= -2\rho\tau/3\ S_{yy} \\
g_7 - g_8 &= -2\rho\tau/3\ S_{xy}
\end{aligned} \tag{16}$$

where it is important to note that this reduction of the equations is not unique. Using the equations (17) it is possible to find expressions for the set of variables g_i in terms of the boundary density, velocity and strain rate. It is therefore clear that the combination of $f_i^{(1)}$ in each g_i cannot be independent and therefore the $f_i^{(1)}$ in that combination cannot all be chosen as 'free' variables i.e. they form forbidden combinations of the link densities.

In order to solve the system of equations (14) we now *choose* three free $f_i^{(1)}$ which (i) are not a forbidden set (in the sense of the discussion above) and (ii) have accessible values (correspond to the f_i streamed onto the boundary node at the previous time step). The set is chosen (subject to (i) above) principally to derive from the bulk, simply in order to promote an exchange of information between boundary and bulk nodes as close as possible to that occurring between bulk nodes. Thus in figure 1, we take pre-collision values of $f_i'^{(1)} = f_i - f_i^{(0)}$, $i = 0, 1, 2$ as free quantities. Accordingly the solution to equations (14), for the particular case represented in figure 1 is

$$\begin{aligned}
f_3^{(1)} &= \tfrac{1}{2}\kappa S_{yy} - f_1'^{(1)} - f_2'^{(1)},\\
f_4^{(1)} &= \tfrac{1}{2}\kappa S_{xy} - \kappa S_{yy} - \tfrac{1}{2} f_0'^{(1)} + 2 f_1'^{(1)} + f_2'^{(1)},\\
f_5^{(1)} &= \tfrac{1}{2}\kappa (S_{xx} + S_{yy}) - \tfrac{1}{2}\kappa S_{xy} + \tfrac{1}{2} f_0'^{(1)} - f_1'^{(1)} = -\tfrac{1}{2}\kappa S_{xy} + \tfrac{1}{2} f_0'^{(1)} - f_1'^{(1)},\\
f_6^{(1)} &= -\kappa S_{xx} - f_0'^{(1)} - f_2'^{(1)},\\
f_7^{(1)} &= \tfrac{1}{2}\kappa S_{xx} + \tfrac{1}{2}\kappa S_{xy} + \tfrac{1}{2} f_0'^{(1)} + f_1'^{(1)} + f_2'^{(1)},\\
f_8^{(1)} &= -\tfrac{1}{2}\kappa S_{xy} - \tfrac{1}{2} f_0'^{(1)} - 2 f_1'^{(1)} - f_2'^{(1)}
\end{aligned} \tag{17}$$

where $\kappa = -2c_s^2 \rho \tau$.

Step (3), the pre-collision values of $f_i^{(1)}$ may now be added to $f_i^{(0)}$ as calculated in equation (17) above, collided and propagated, to complete the evolution of our boundary site.

4. Results

We applied the boundary algorithm described in the last section to channel flow, with rest boundaries $u_{0x} = u_{0y} = 0$ located at $y = 0^-$, W^+ with the width of the channel, W, taken to be 20. Periodic boundaries were applied in the x-direction and forced by a uniform pressure gradient in the x-direction [4]. Figure 2 shows the normalized difference between the measured steady-state flow profile $v_m(y)$ and the corresponding (parabolic) analytic solution $v_{th}(y)$ as a function of y:

$$\varepsilon_r = \left| \frac{v_m(y) - v_{th}(y)}{v_{th}(y)} \right|, \qquad y \neq 0, \tag{18}$$

as obtained using first-order accurate bounce-back boundary conditions (dashed curves) over a range of collision parameter $1/\tau = 0.37, 0.5, 1.0, 1.5$ and 1.8. Figure 2 also shows the results of an equivalent set of simulations using the lattice closure algorithm of the last section (solid curves). These results clearly reveal the short-comings of the first-order accurate technique as a reduction in the accuracy of the solution close to the lattice boundaries. The data of figure 2 were obtained for constant lattice resolution, constant forcing and variable Reynolds number. The accuracy of the solution obtained using our closure algorithm is, by contrast, uniform and second order across the whole width of the simulation and over the range of Reynolds number.

To demonstrate that our boundary closure is instantaneously correct, we consider a lattice fluid initially confined at rest (momentum densities set to $f_i^{(0)}(\rho, \mathbf{0})$) between two planes $y = 0^-$, W^+. The upper plate is impulsively started at $t = 0^+$ to velocity $u_{0x} = u_0$, $u_{0y} = 0$ (in lattice units) through equation (13). For this situation the Navier–Stokes equation may be

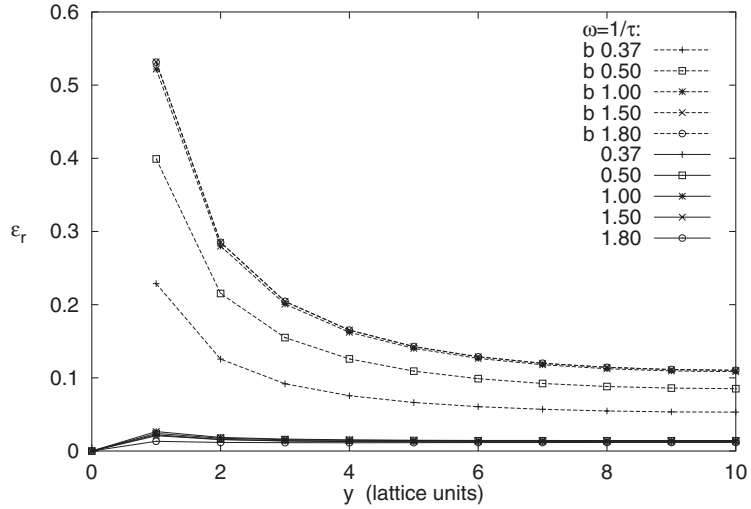

Figure 2. Comparison of the normalized error (difference between measured and analytical parabolic profiles) at steady state, for traditional bounce-back boundary conditions (dashed curves) and the closure algorithm introduced here (solid curves). The data represent a range of collision parameter: $1/\tau = 0.37$, 0.5, 1.0, 1.5 and 1.8 denoted by +, □, ∗, × and ○ respectively, for both cases. The duct width (resolution) was 20. Bounce-back boundary accuracy varies significantly with Reynolds number (value of τ). In comparison the smaller relative error associated with the new lattice closure scheme shows significantly less variation.

reduced to a one-dimensional diffusion equation with inhomogeneous boundary conditions. Seeking a solution in the form of a steady state with separable transient yields

$$v_x(y,t) = \frac{u_0}{W}\,y + \frac{2u_0}{\pi}\sum_m \frac{(-1)^m}{m}\sin\left(\frac{m\pi y}{W}\right)\mathrm{e}^{-m^2\pi^2\bar{t}}, \qquad \bar{t} = \frac{\nu t}{W^2}. \tag{19}$$

Here $\bar{t}$ represents a *dimensionless* time parameter allowing direct comparison between analytic and measured profiles.

Snapshots of the developing flow across the whole width of the duct, obtained for three values of discrete time $t = 10$, 100, 1000 and collision parameter, $1/\tau = 0.6$, 1.0, 1.6, are shown in figure 3(*a*) (symbols), alongside the corresponding analytical solution (19) (curves). The data in figures 3 were obtained with the lattice resolution and Reynolds number fixed, the latter being conserved by adjusting the moving plate velocity; they are presented in pairs, characterized by the same value of $\bar{t}$. Clearly the agreement between the two is excellent, even down to a very small number (ten) of simulation time steps. Note, moreover, that the lattice edge velocity (velocity measured on the lattice boundary nodes) is exactly the assigned velocity.

The data of figure 3(*b*), showing the relative error ε_c

$$\varepsilon_c = \frac{v_m(y) - v_x(y)}{u_0}, \tag{20}$$

evaluated at different flow stations y, for the profiles of figure 3(*a*), reveal that the relative error generally increases as the dimensionless time $\bar{t}$ decreases. Even ignoring the fact that, at $t = 0^+$, the measured lattice velocity y gradient cannot be infinite (its analytical value), the profiles of figure 3 show encouraging agreement with the analytical result, down to very short times. Naturally for low viscosities ($1/\tau$ approaching 2), the diffusion of velocity from the upper (loaded) plate is slower. Accordingly the finite-difference approximation for the velocity

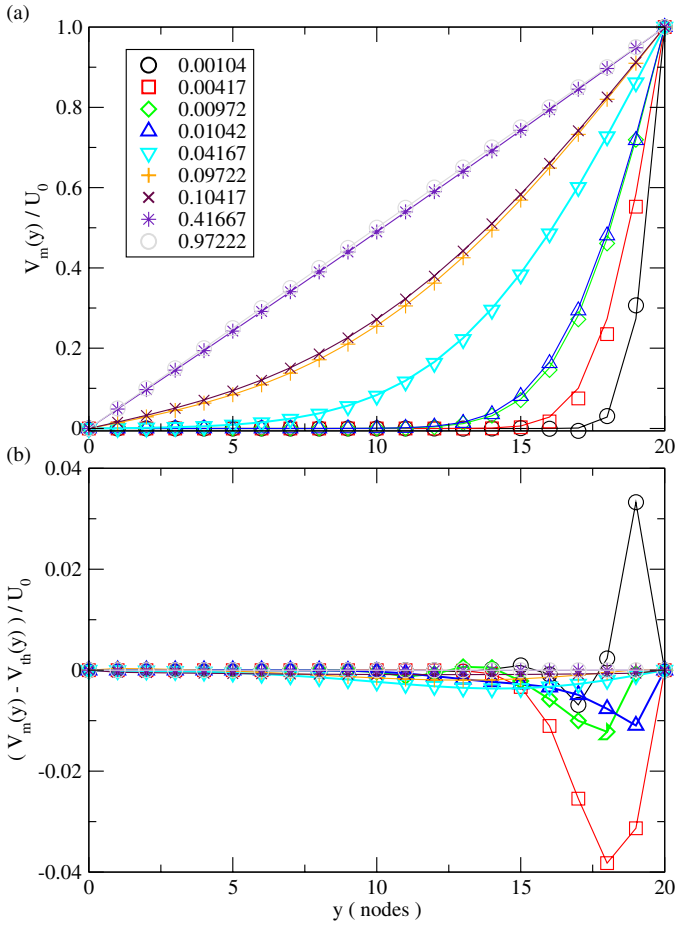

Figure 3. (*a*) Impulsively started Couette flow profiles obtained for $Re = 0.024$ and simulation width (resolution) $W = 20$. The Reynolds number was maintained constant by adjusting the moving plate velocity. Symbols show the normalized, measured profile; curves show the corresponding analytical profiles characterized by the same value of $\bar{t}$. (*b*) The relative error, as given by equation (20) as a function of distance y across the duct, for the data of figure 3(*a*).

(This figure is in colour only in the electronic version)

y gradient at the boundary (plate) is poor, as is the convergence of the analytical solution (19) (due to the Gibbs phenomenon), both of which considerations affect the agreement at very small values of $\bar{t} = \nu t / W^2$, that is in the high-flow-gradient regime.

Nevertheless in all cases the velocity gradients do not change discontinuously near the lattice-edge. Moreover, the relative error associated with the boundary is similar to that associated with the bulk scheme.

5. Conclusion

In this summary account we have set out and validated an adaptable method for closing an LB simulation lattice by calculating appropriate values for the set of missing momentum densities. Our algorithm is demonstrably accurate, flexible and instantaneously correct.

Furthermore, as Ginzbourg and d'Humières [3] have effectively demonstrated with their LSOB method, the essential idea we use will generalize to any linearized LB scheme and boundary orientation, provided one is prepared, in the language of the present work, to extrapolate the fluid density onto the Dirichlet boundary. Without similar modification the present approach would generalize only to a boundary orientation for which the sum of the missing momentum densities can be determined, through an identity like equation (13) above.

Our method could, in future, be further generalized to allow the simulator the freedom to place a boundary with known velocity distribution at any distance $y = h(x)$: $0 < h(x) < |c|$ off-lattice, bringing precise control of the simulation boundary within the scope of the method.

Thanks are due to Professor D d'Humières for comments on our original manuscript.

References

[1] Chen S, Martinez D and Mei R 1996 *Phys. Fluids* **8** 2527
[2] Gallivan M A, Noble D R, Georgiadis J G and Buckius R O 1997 *Int. J. Numer. Methods Fluids* **25** 249
[3] Ginzbourg I and d'Humières D 1996 *J. Stat. Phys.* **84** 927
[4] Halliday I, Hammond L A, Care C M, Good K and Stevens A 2001 *Phys. Rev.* E **64** 011208
[5] He X Y, Zou Q, Luo L S and Dembo M 1997 *J. Stat. Phys.* **87** 115
[6] Hou S, Zou Q, Chen S, Doolen G D and Cogley A C 1995 *J. Stat. Phys.* **118** 329
[7] Inamuro T, Yoshino M and Ogino F 1995 *Phys. Fluids* **7** 2928
[8] Kim I C 2000 *KSME Int. J.* **14** 84
[9] Noble D R, Chen S, Georgiadis J G and Buckius R O 1995 *Phys. Fluids* **7** 203
[10] Qian Y H, d'Humières D and Lallemand P 1992 *Europhys. Lett.* **17** 479
[11] Skordos P A 1993 *Phys. Rev.* E **48** 4823
[12] White D M, Halliday I, Care C M and Stevens A 1999 *Physica* D **129** 68
[13] Zou Q and He X Y 1997 *Phys. Fluids* **9** 1591